Available online at www.sciencedirect.com
ScienceDirect
Journal of Power Sources 163 (2006) 330–338
JOURNAL OF POWER SOURCES
www.elsevier.com/locate/jpowsour

Combinatorial screening of thin film electrocatalysts for a direct methanol fuel cell anode

James S. Cooper *, Paul J. McGinn [1]

Department of Chemical and Biomolecular Engineering, Center for Molecularly Engineered Materials, University of Notre Dame, Notre Dame, IN 46556, United States

Received 10 July 2006; received in revised form 18 August 2006; accepted 15 September 2006
Available online 1 November 2006

Abstract

The Pt-Ru-W and Pt-Ru-Co ternary alloy systems were investigated for use as anode catalysts in direct methanol fuel cells. Plasma sputtering through shadow masks was used to deposit discrete composition combinatorial libraries. Post-deposition annealing promoted multilayer homogenization, with interdiffusion of the layers confirmed by X-ray diffraction. The short term methanol oxidation activities of the different compositions were compared in parallel by cyclic voltammetry with a multichannel electrochemical cell. It was found that the optimum composition changed from initial to final tests. Initially $Pt_{25}Ru_0W_{75}$ and $Pt_{17}Ru_{17}Co_{66}$ outperformed the best binary Pt-Ru catalyst by 3× and 20×, respectively. Cycling the potential at 60 °C was found to change the performance of some compositions. The performance of Pt-Ru binary catalysts were improved by this conditioning and the optimum ternary compositions shifted to $Pt_{44}Ru_{12}W_{44}$ and $Pt_{12}Ru_{50}Co_{38}$. The optimum Pt-Ru-W composition had a peak methanol oxidation current density that was 1.5× more than the best Pt-Ru binary composition. The peak methanol oxidation current density of the best Pt-Ru-Co composition was 2.5× more than the best Pt/Ru binary composition and had a substantially lower onset potential.
© 2006 Elsevier B.V. All rights reserved.

Keywords: Direct methanol fuel cell (DMFC); Electrocatalysis; Methanol oxidation reaction; Cyclic voltammetry; Multichannel microarray; Pt-Ru-W-Co

1. Introduction

Direct methanol fuel cells (DMFC) are a promising, portable, low temperature power source. A contemporary review of recent research notes achievements of enhanced power densities and efficiencies, but also concedes that for commercialization the DMFC must incorporate catalysts that are cheaper, less prone to poisoning and more catalytically active [1]. Many research efforts have been directed at improving poison resistance and reducing the overall Pt content in the catalysts [2,3]. Early work carefully studied methanol oxidation on platinum surfaces; pure [4] and altered by a second element like Au [5], Sn [6], Ru [7,8], and many others [9]. This has been followed by combinatorial investigations that covered larger composition fields with some successful and exciting discoveries [10,11]. Despite the significant investigations $Pt_{50}Ru_{50}$ has remained the most commonly used catalyst in the anodes of direct methanol fuel cells [1].

The progress made in improving Pt alloys came from a thorough investigation of methanol oxidation on various catalyst surfaces in particular Pt-Ru alloys. The current understanding is that the methanol oxidation reaction can proceed via multiple pathways and is influenced by a myriad of variables [12]. Despite the complexity of the reaction, two crucial steps have been defined for Pt alloy catalysts; the adsorption of methanol and the oxidation of carbon monoxide [13]. Although the Ru is believed to dilute and reduce methanol adsorption sites, it is vital for the oxidation of carbon monoxide. There are two theories that explain ruthenium's role during this step. The bifunctional mechanism portrays ruthenium atoms as the optimum site for water adsorption and serves as a donor of oxygen to react with the surface bound carbon monoxide [14]. In contrast the ligand model implies that the presence of ruthenium alters the platinum's d-band occupancy, lowering the activation energy for carbon monoxide oxidation directly at the Pt site [15]. Ruthenium could be aiding platinum by either or both of these methods. The complex nature of the reaction means ruthenium's exact role cannot

* Corresponding author. Tel.: +1 574 631 5692; fax: +1 574 631 8366.
E-mail addresses: jcooper1@nd.edu (J.S. Cooper), mcginn.1@nd.edu (P.J. McGinn).
[1] Tel.: +1 574 631 6151.

0378-7753/$ – see front matter © 2006 Elsevier B.V. All rights reserved.
doi:10.1016/j.jpowsour.2006.09.028

be completely specified for every possible situation. This complexity also means that the possibility of further improvement in alloy composition is possible. The ideal catalyst should provide plentiful sites for methanol adsorption without being susceptible to poisoning by any intermediate products.

Most examinations of Pt alloy systems have been limited to binary systems because of the experimental difficulties involved in trying to examine a wide range of ternary alloys [16]. However, modern materials processing techniques have made it more feasible to explore new catalyst compositions through a combinatorial approach [17]. Combinatorial libraries have been fabricated via a variety of methods, including physical vapor deposition techniques such as sputtering [18,19], or less commonly by techniques such as electro-deposition [20] or gel transfer [21]. Such libraries have been characterized by many different screening techniques including fluorescence imaging [22–24], scanning electrochemical microscopy [25], multiarray half cell [26] and multiarray fuel cell [27]. There are benefits and disadvantages with each method [28], with the criteria that define the optimum combinatorial method [29] for a particular materials problem still the subject of discussion. In the present study, we use a thin film combinatorial approach based on sputtering of discrete composition libraries. Parallel potentiostatic testing was used to screen these libraries to identify anode catalyst compositions that merit more thorough testing in a true fuel cell environment.

2. Experimental

2.1. Library synthesis

The sputtering system used in this work includes five fixed 2 in sputtering sources, with computer controlled shutters. Between the guns and the substrate holder is a carousel that holds twelve 2 in diameter masks. Rotation of the mask carousel and substrate holder allows the substrate to be positioned above any of the guns with any mask positioned between. A computer program sequentially selects gun and mask combinations to deposit a series of multilayer samples with varying compositions on the substrate. The system is described in more detail elsewhere [30].

Building a discrete composition library starts by using photoresist to develop a pattern of titanium nitride leads and pads on a 2 in silicon wafer, Fig. 1a. In the center of the wafer the photoresist pattern defines 76 pads on which the discrete composition library members are deposited. These capture pads are hexagonal (0.026 cm^2) with a nearest neighbor distance of 1.6 mm. Around the periphery of the wafer there is a ring of electrical contact pads that are the connection points to the multichannel potentiostat. Finally, a network of electrical traces connects each hexagonal capture pad with its respective circular contact pad. A non-symmetric marker is included on the left of the pattern to help with orientation and alignment issues.

The discrete compositions that rest on the hexagonal TiN capture pads are formed by depositing through six binary shadow masks depicted in Fig. 1b. The 32 black hexagons in each mask indicate the openings through which material deposition would occur. The holes in the masks are aligned in a geometric pattern

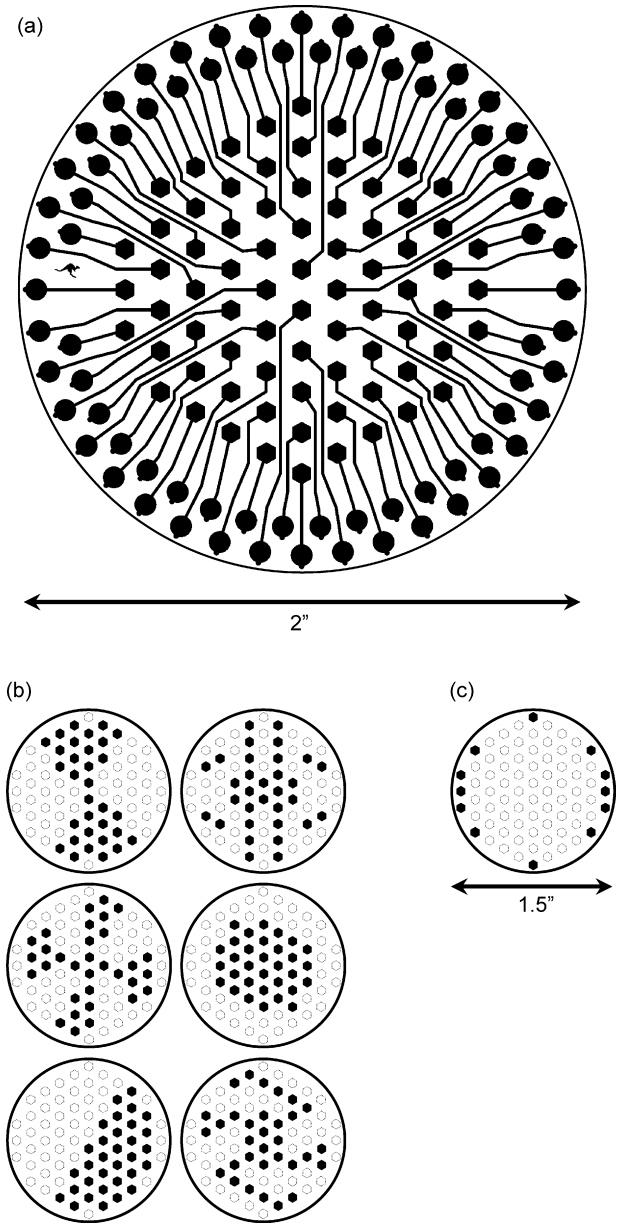

Fig. 1. (a) Photoresist pattern that defines hexagonal composition pads, circular contact pads and a network of traces connecting them; (b) six combinatorial shadow masks that each have 32 hexagonal holes, each hole is aligned with 1 of 63 discrete composition pads and (c) the 12 periphery pads are captured by a 7th shadow mask usually with a control composition like pure Pt.

above 63 positions on the substrate. Typically, these masks will be used in a layer by layer deposition sequence that builds up 49 unique ternary compositions. This common deposition sequence results in reasonable coverage of a ternary phase field. Other special deposition sequences can concentrate more compositions around an area of interest. Outside of the combinatorial pattern are 12 composition pads that are captured with a 7th mask, Fig. 1c. A fixed reference composition, usually Pt, is deposited at these 12 locations to permit easy comparison between libraries. After deposition 75 of the 76 hexagonal pads contain multilayer thin films, each one a sample of a specific catalyst composition.

The multilayer thin films require annealing to homogenize their laminate structures into a form that will ideally be equiva-

lent to an annealed bulk alloy sample. Annealing may not result in the same surface composition as other techniques, such as co-sputtering [19]. Studies on Pt alloys showed that annealing under vacuum generally resulted in a monolayer skin that was Pt rich, but alloys annealed in reducing conditions had surfaces consistent with the bulk [31–35]. Samples in this study were annealed ex situ after deposition in a 10^{-6} Torr vacuum. The annealing schedule was 550 °C for 4 h followed by a rapid high temperature anneal at 900 °C for 5 min.

Annealing to achieve interdiffusion could also lead to Si diffusing through the thin film structure and contaminating the surface. Two diffusion barriers slow the migration of Si into the film; the first is a 0.3 μm thick SiO_2 layer thermally grown on the wafer before any processing. Secondly, the patterned, inert TiN base also acts as a diffusion barrier. Auger analysis has confirmed that the surface remains free of Si or Ti after annealing.

Structure characterization is performed with a modified Scintag X1 advanced diffraction system. Capillary optics (XOS Inc.) focus the Cu Kα radiation to a spot size of 5 mm^2 at the specimen surface. A homemade computer controlled stage moves the specimen, sequentially aligning library compositions with the beam. Typically a theta–theta scan was performed on each catalyst sample from $2\theta = 32°$ to 46° at 0.01° s^{-1}. With these specifications an entire library is characterized in a total of 33 h. X-ray diffraction was done before and after annealing, confirming that heat treatment altered the initial laminate structure.

2.2. Electrochemical characterization

Electrochemical testing was performed with a commercial multielectrode potentiostatic system (Scribner Associates Model 900B Multichannel Microelectrode Analyzer (MMA)) in conjunction with a specially designed electrochemical cell. This system can control the potential and measure the respective currents from up to 100 combinatorial library members. A cutaway schematic drawing of the cell is shown in Fig. 2. Leads run from the MMA to a ring assembly of gold pogo probes (Everett Charles Inc.) that are pressed down on the ring of TiN contact pads. A 38 mm diameter glass cylinder and silicone o-ring press down on the wafer, separating the catalyst library pads and the

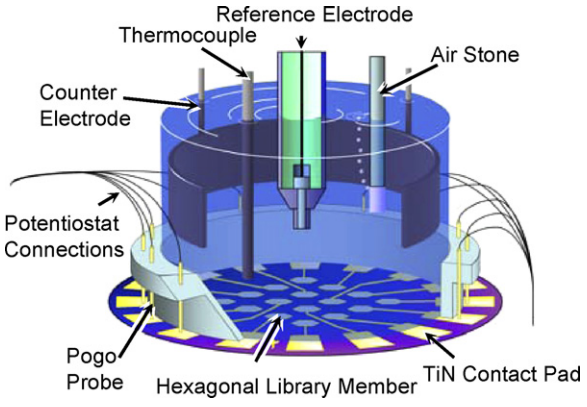

Fig. 2. Schematic drawing of the assembled electrochemical cell. Note that a simple 16 member library is shown for clarity.

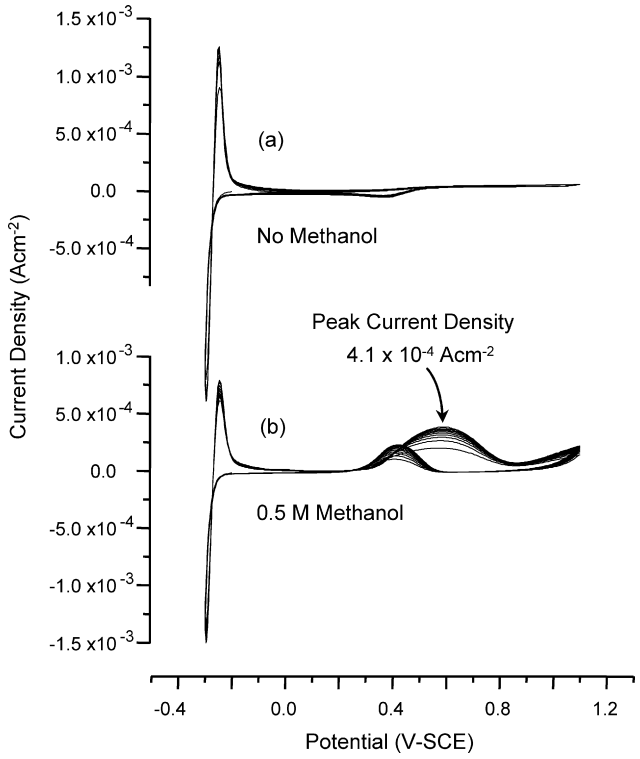

Fig. 3. Sample cyclic voltammetry curves recorded from a $Pt_{92}Ru_8$ catalyst pad that show the current–potential response in (a) clean electrolyte and (b) with 0.5 M methanol. Scan rate was 10 mV s^{-1} in 0.5 M H_2SO_4 cycled 10 times at 20 °C.

electrolyte from the contact pads. A plastic lid with a Teflon gasket (not shown in Fig. 2) screws down on the assembly, fixing the entire cell in place. Once the wafer, pogo pins, glass cylinder and Pt coated Nb counter electrode (that runs completely around the periphery of the cell) are assembled, the interior of the cell is triple rinsed with 18 milli-q water and then filled with 40 mL 0.5 M H_2SO_4 (made from 96.6% pure H_2SO_4, Fisher Scientific). A type J stainless steel thermocouple, calomel reference electrode (Cole-Palmer Inc.) and type C air stone (Ace Glass Inc.) are inserted into the lid and suspended in the electrolyte. The counter electrode and the junction of the reference electrode are 17 mm above the wafer, while the thermocouple tip is ∼2 mm from the wafer surface.

For the methanol oxidation reaction dry nitrogen was passed through the air stone until a stable open circuit potential was achieved, which usually required at least 10 min. The cell potential at all of the catalyst pads was then set and held at −0.2 V-SCE for an additional 10 min before testing. Testing began by acquiring cyclic voltammograms at room temperature between −0.3 and +1.1 V-SCE, ramping at 10 mV s^{-1}, until a stable curve was reproducibly measured from all of the catalyst pads. This usually required 10–20 cycles. A sample cyclic voltammetry curve in clean electrolyte is shown in Fig. 3a. Note that the reported current density is based on the geometric area of the sample pad (0.026 cm^2) and not the active area. The active area of platinum surfaces is usually determined by examining a monolayer adsorption during a potential sweep [36–38]. The present combinatorial approach necessitates reporting currents from widely

varying compositions, including some with no platinum at all. These compositions have an overpotential for the adsorption of H^+ or other species and their active area cannot be defined in situ by these methods. Other methods to determine roughness, such as DEMS [39] or STM [40] are not compatible with the present combinatorial testing approach.

For screening of methanol oxidation activity, the potential was again held at −0.2 V-SCE while 0.82 mL methanol (99.9% pure, Fisher Scientific, equivalent to 0.5 M in 40 mL solution) was introduced into the electrolyte. The potential was maintained at −0.2 V-SCE for a further 270 s to allow the solution to homogenize and the measured currents to stabilize. Following the introduction of the methanol, the potential was again swept from −0.3 to 1.1 V-SCE at 10 mV s^{-1} until reasonably stable curves were again measured from all of the catalyst pads. Fig. 3b shows the cyclic voltammogram of an active catalyst with the methanol oxidation reaction beginning at 0.3 V-SCE and peaking at 0.58 V-SCE. The potential where the methanol oxidation reaction started and the current density at the peak of the reaction were used to compare the different compositions. Although these quantities are characteristic of short term behavior, they are reasonable indicators of whether a catalyst composition may be beneficial in the methanol oxidation reaction.

Immediately before and after electrochemical testing each of the catalyst pads was photographed (Olympus DP70 microscope with BX70 stage). These images were used to determine the corrosion resistance of the thin film catalysts. Libraries were tested at room temperature, 40 and 60 °C. The higher temperatures were achieved with a foil-type resistive heater (Minco) positioned under the wafer. The cell was deaerated and the potential held at −0.2 V-SCE for 10 min before any heating procedure started. The total time to complete a test at one temperature was approximately 4 h. Thus, every library was immersed in 0.5 M H_2SO_4 for approximately 20 h (testing at 20, 40, 20, 60 and 20 °C again). During this time some catalyst compositions would corrode. The extent of corrosion was assessed by image analysis of the micrographs to determine how much of each catalyst's initial 0.026 cm^2 surface area was lost.

Extensive characterization of the cell design was performed prior to the reported experiments. For example, measurements were made on special libraries with the same composition at every location. With these libraries it was found that the electrolyte and contact lead resistances were negligible. Ternary libraries were examined only after verifying the reliability of the data. Compositions were ranked based on their onset potentials and peak methanol oxidation current densities for a few reasons. The onset potential was examined because it is not influenced by any change in the surface roughness. Previous testing we have performed showed there was a strong correlation between the peak current density and the current density observed after a 5 min chronoamperic experiment at 0.5 V-SCE. This corroborates reports of a reasonable connection between short term performance measured in an electrochemical cell environment and results from longer steady state tests [23,26,41–43] or from actual fuel cells [10,28]. A longer chronoamperic experiment would measure the current under steady state conditions and would theoretically be closer to fuel cell operating conditions. Unfortunately, the decay of the current with time increases the possibility of systematic errors misleading the results. The peak methanol oxidation current densities have less systematic error than the chronoamperic currents making them the better measurement to judge relative catalyst performances.

This screening test is only designed to recognize promising compositions. This is a simple test that compares methanol oxidation properties in an environment that avoids complex fuel cell testing issues like particle size, distribution, loading, support, degradation, etc. Confirmation that these compositions are good DMFC catalysts is a separate work based on powder synthesis and many other testing techniques. A thin film composition that has a low onset and a strong current density in the short term may excel in a fuel cell. If it does then further analysis will be carried out on the high surface area powder to confirm this. These thin film libraries were only intended to quickly identify compositions that may work well in a fuel cell.

3. Results and discussion

3.1. X-ray

The annealing regime promoted interdiffusion with each composition changing from a laminate nanostructure to a homogenous alloy. Fig. 4a and c depict the spectra of representative Pt-Co and Ru-Co binary compounds, respectively. A spectrum for a pure Pt sample can be seen at the top of Fig. 4a with only the (1 1 1) peak discernable. The lack of other peaks is due to the film growing in a textured manner. TiN (1 1 1) and (2 0 0) peaks from the substrate were present in all of the scans at $2\theta = 36.58°$ and 42.59°. The strong relative intensity for the majority of samples made the TiN peaks barely discernable from the background. However, Co rich samples had a relatively low intensity, so in these samples the TiN peaks are quite prominent and labeled appropriately in Fig. 4a and c.

The 2θ peak shift across the entire phase field is depicted in Fig. 4b. Each circle in Fig. 4b indicates the 2θ measured for that specific composition with the dark to light shading indicative of the value from 40.0° to 44.2°. The background has been shaded using an averaging function to highlight the trend. The majority of samples appear to have formed alloys with no sign of the intermediate compounds $CoPt_3$ or CoPt. The ternary representation in Fig. 4b shows that the change in 2θ is linearly proportional to the composition, consistent with expectations from Vegard's law. Between $Pt_{20}Ru_{80}Co_0$ and $Pt_{57}Ru_{43}Co_0$ there were some signs of a Pt structure coexisting with Ru and Pt-Ru alloy phases. This is partially consistent with the binary phase diagram [44] that predicts a two phase region between $Pt_{38}Ru_{62}$ and $Pt_{20}Ru_{80}$. Note that it is only the 2θ of the alloy phase that is replotted in Fig. 4b.

3.2. Electrochemical testing

3.2.1. Pt-Ru binary

Pt-Ru is the standard alloy used as the anode electrocatalyst in direct methanol fuel cells. Our goal is to replace Pt-Ru with a catalyst that out-performs it and/or is less expensive.

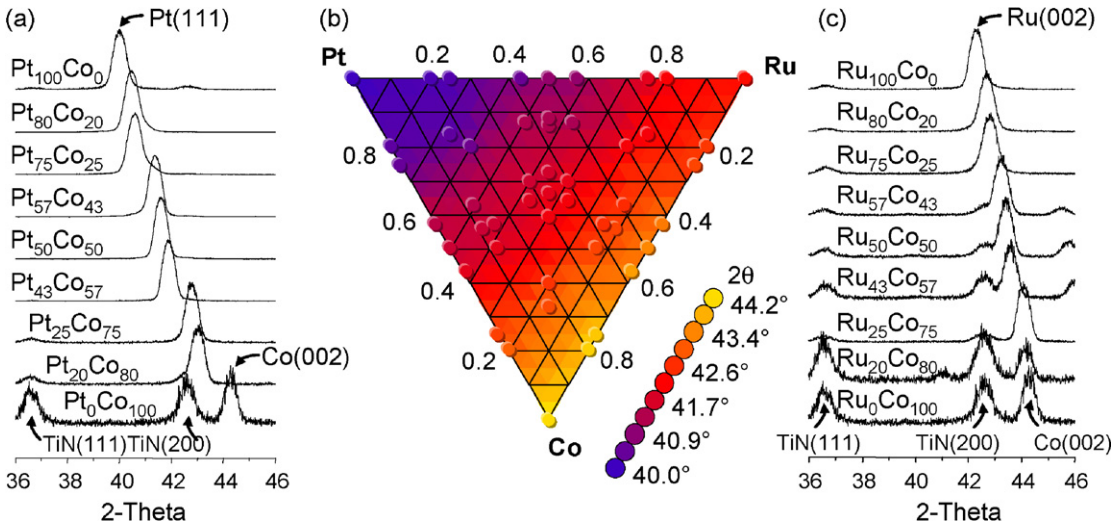

Fig. 4. (a) X-ray diffraction scans of the binary combinations of Pt and Co; (b) ternary plot with the 2θ distortion of the strongest peaks Pt(1 1 1), Ru(0 0 2) and Co(0 0 2) and (c) X-ray diffraction scans of the binary combinations of Ru and Co.

We first characterized Pt-Ru compositions to establish a standard for comparison with novel compositions. The initial Pt-Ru library tested included compositions that spanned from pure Pt to pure Ru. The first electrochemical test at room temperature showed negligible activity from all samples. Testing at higher temperatures "activated" some samples, resulting in improved peak current densities that remained regardless of the subsequent testing temperature. A library that had been previously tested at 60 °C was retested at room temperature with the resultant current density at the peak of the methanol oxidation reaction plotted in Fig. 5. Where there are multiple data points for the same composition the average is displayed with error bars determined by the standard deviation. The line in Fig. 5 is a Gaussian fit that highlights the trend and helps define an optimum composition at $Pt_{90}Ru_{10}$. The trend of near zero activity continues from $Pt_{50}Ru_{50}$ all the way to pure Ru.

The best Pt-Ru composition for methanol oxidation reported in the literature varies depending on several factors. Tests on carbon supported high surface area catalyst nanoparticles tend to show $Pt_{50}Ru_{50}$ as the best composition [45,46]. This conflicts with electrochemical surface studies of relatively flat metallic surfaces that tend to report a Pt rich optimum composition between $Pt_{90}Ru_{10}$ and $Pt_{80}Ru_{20}$ [19,35,47,48]. However, even this "flat surface optimum" has been seen to shift to higher Ru concentrations $\sim Pt_{70}Ru_{30}$ at higher temperatures [33,41]. Our study found the optimum composition at all temperatures was $Pt_{90}Ru_{10} \pm 5$ at% in agreement with most of the "flat surface" studies. Why these results differ from the results achieved with high surface area particles remains an open question. There is a variety of theories that explain the discrepancy, ranging from surface segregation during nanoparticle fabrication [49] to empirically derived reaction mechanisms [50], but nothing definitive has been established.

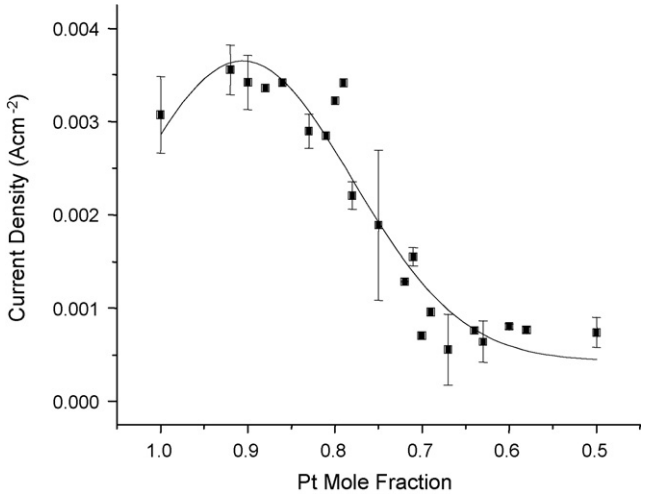

Fig. 5. Peak methanol oxidation current densities measured from conditioned Pt-Ru compositions during the 10th sweep of a cyclic voltammetry experiment, 10 mV s^{-1} scan rate in 0.5 M H_2SO_4, 0.5 M methanol at 20 °C.

The performance improvement that occurred after elevated temperature testing seen in this work is not fully understood. Proton exchange fuel cells are generally conditioned before testing but this is principally to ensure the membranes are hydrated [51]. There have been some reports of the conditioning process altering the catalyst, usually with ruthenium oxide being reduced [52]. There are many possible processes that could occur in our thin film libraries at the elevated temperatures. There could be a corrosion effect, an acid induced surface modification, reduction of an oxide or the removal of stubborn organic contaminants [53]. Determining the exact mechanism is part of an ongoing study.

3.2.2. Pt-Ru-W

The first test on an unconditioned Pt-Ru-W library showed a weak response from a wide range of compositions. The best performing composition was $Pt_{25}Ru_0W_{75}$ with a current density of 5.7×10^{-4} A cm^{-2}. The majority of the other compositions had a current density less than 2×10^{-4} A cm^{-2} with the exception of the W-Ru compositions which showed no response. Testing at 40 and 60 °C conditioned the library and resulted in a strong response from a few compositions. Fig. 6a shows the peak

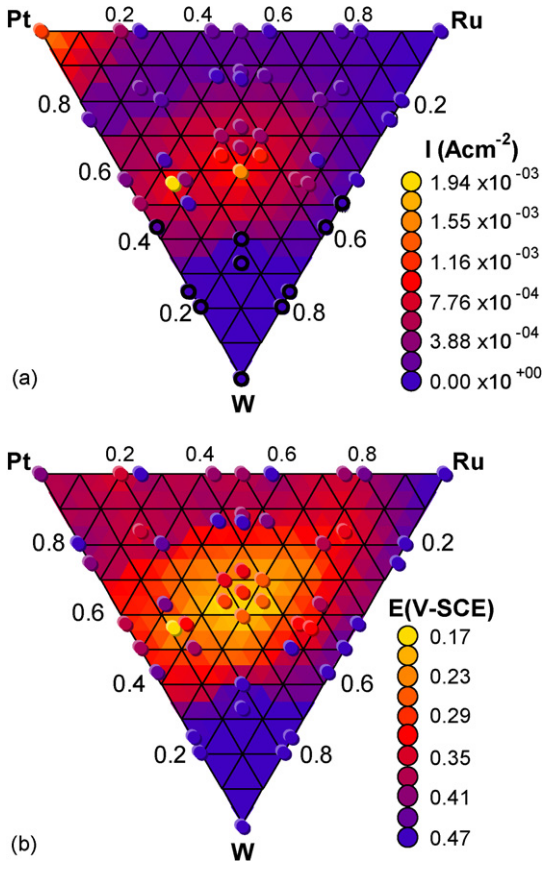

Fig. 6. (a) Peak current densities and (b) onset potentials of methanol oxidation for the Pt-Ru-W system. Measurements taken during the 10th forward scan at 10 mV s^{-1} in 0.5 M H_2SO_4, 0.5 M methanol at 20 °C. Black rings in (a) indicate compositions that lost more than 50% of their surface area during testing.

methanol oxidation current density for a conditioned library tested again at 20 °C. Extremely high conversion occurred in a narrow range, with the best composition $Pt_{44}Ru_{12}W_{44}$ achieving a current density of 1.9×10^{-3} A cm^{-2}. This is 1.5× more than the average Pt catalyst current density of 1.2×10^{-3} A cm^{-2}. Note that to cover the ternary field a library with reasonably wide steps between compositions was required. For this reason, $Pt_{90}Ru_{10}$ could not be represented and the ternary performance is compared to either pure Pt or $Pt_{80}Ru_{20}$.

Strong current densities for tungsten alloys have been previously reported as being due to preferential dissolution that leaves a rougher surface [18]. The most active composition in our libraries also had a 0.2 V lower onset potential than the best Pt-Ru binary composition, Fig. 6b. This implies that the improved performance was due to an altered reaction mechanism and not merely a change in electroactive area. This does not mean that all tungsten alloys are perfectly stable. Some pads showed signs of deterioration after testing; those that had less than 50% surface area after testing are indicated with black rings in Fig. 6a. Obviously, tungsten rich compositions are unstable in the acidic environment. Automated optical microscopy was used to photograph all of the pads after electrochemical testing. Fig. 7 shows representative optical micrographs of varying levels of pad degradation. Changes ranged from no degradation, to pads that disappeared completely. The mechanism of corrosion could have been galvanic, spalling due to a thin film stress issue or simply electrochemical dissolution at the extreme test potentials. These types of corrosion would probably not be an issue in a true fuel cell environment, but their poor performance has eliminated these compositions from further investigation.

The best performing composition observed in the present work, $Pt_{44}Ru_{12}W_{44}$, does not agree with the optimum com-

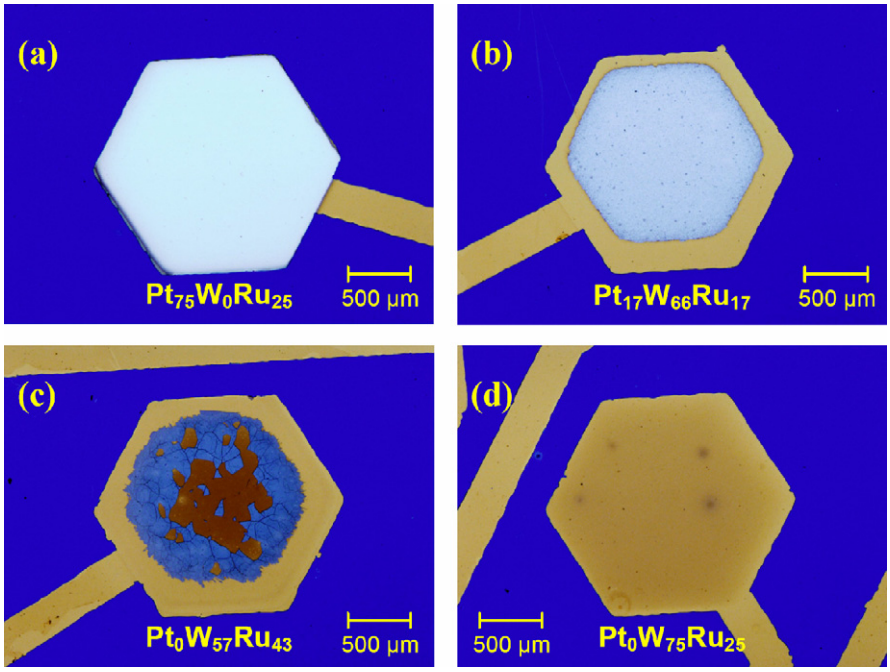

Fig. 7. The different degrees of corrosion afflicting Pt-Ru-W test pads after 4 days testing: (a) unaffected; (b) partial corrosion; (c) partial corrosion and spalling and (d) complete failure.

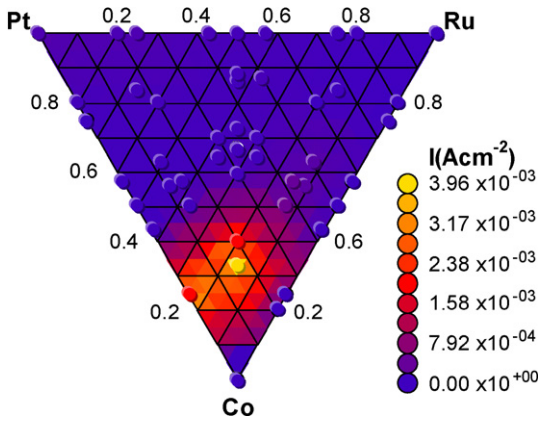

Fig. 8. Peak current densities of methanol oxidation for the Pt-Ru-Co system that has not been previously tested and is not conditioned. Current densities measured during the 10th forward scan at 10 mV s^{-1} in 0.5 M H_2SO_4, 0.5 M methanol at 20 °C.

positions found by other groups. Holleck et al. [54] found $Pt_{82}W_{18}$ was better than pure Pt, but that $Pt_{53}Ru_{32}W_{15}$ was the best. Tanaka et al. [42] found $Pt_{80}Ru_{20}$ was favorable, but $Pt_{65}Ru_{20}W_{15}$ was an even better performer. Umeda et al. [55] found $Pt_{65}Ru_{20}W_{15}$ to be far superior to pure Pt and somewhat better than $Pt_{80}W_{20}$, but their investigation was not focused on finding an optimum composition. Jusys et al. [39] also looked at a single composition and found the activity of $Pt_{54}Ru_{39}W_7$ similar to the PtRu produced commercially by E-TEK. Goetz and Wendt [56] prepared catalysts by the Bönnemann method maintaining a constant ratio of Pt and Ru but varying the W concentration. They found that the optimum composition was $Pt_{28}Ru_{28}W_{44}$ but acknowledged this would probably change with a differing synthesis method. In other studies, our group [57] investigated composition spread thin film libraries in the Pt-Ru-W system with a scanning electrochemical microscope and determined that $Pt_{30}Ru_{35}W_{35}$ was the optimum composition to oxidize hydrogen in the presence of carbon monoxide. However, it has also been recognized that the long term functionality of tungsten alloys may be limited. Most groups have reported a degradation of catalytic activity due to the corrosion of the tungsten. The complete deterioration of samples with more than 75% tungsten partially confirms that corrosion affects tungsten alloys. On the other hand, the onset potential of $Pt_{44}Ru_{12}W_{44}$ was substantially lower, and that is a parameter that would not be duly affected by a changed electroactive area.

3.2.3. Pt-Ru-Co

Examination of the Pt-Ru-Co system showed that the optimum composition also changed as testing proceeded. The first room temperature test, while the library was in an unconditioned state, showed little to no response from every composition except $Pt_{17}Ru_{17}Co_{66}$, Fig. 8. That composition responded so strongly it exceeded the system's current measurement limits. Extrapolation of its cyclic voltammetry curve implies it would have a peak methanol oxidation current density of 3.96×10^{-3} A cm^{-2}. This was 20× more than the unconditioned platinum on the same library. This composition also had an onset potential that was 0.2 V lower than the best Pt-Ru composition. However, the promising performance of $Pt_{17}Ru_{17}Co_{66}$ diminished with subsequent tests at higher temperatures.

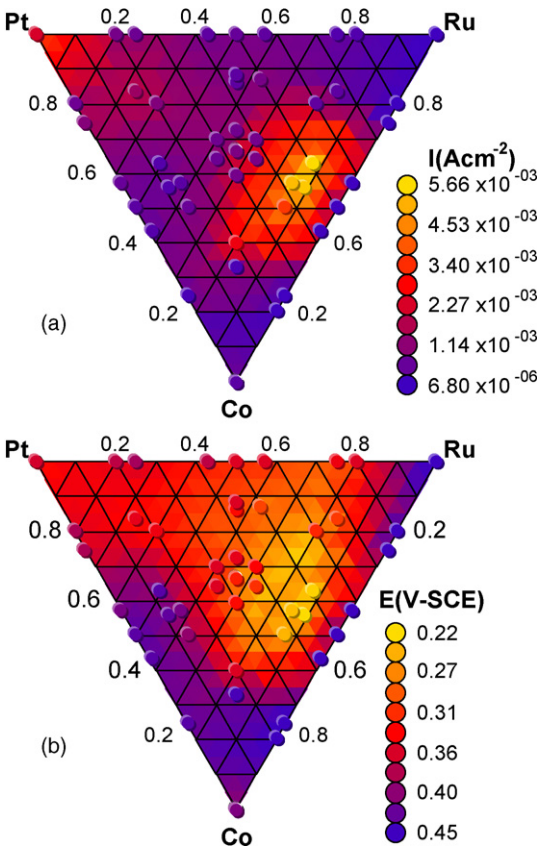

Fig. 9. (a) Peak current densities and (b) onset potentials of methanol oxidation for the Pt-Ru-Co system that has been conditioned by a previous test at 60 °C. Current densities measured during the 10th forward scan at 10 mV s^{-1} in 0.5 M H_2SO_4, 0.5 M methanol at 20 °C.

As expected from prior experiments, 60 °C testing conditioned the library and the Pt rich, Pt-Ru alloys responded more favorably than they had at room temperature, Fig. 9. Interestingly the compositions around $Pt_{12}Ru_{44}Co_{44}$ were also activated by this conditioning with current densities so strong that extrapolation was again required to estimate their true value. $Pt_{12}Ru_{50}Co_{38}$ was the best composition generating a peak methanol oxidation current density of 5.6×10^{-3} A cm^{-2} that was 2.5× more than the average Pt current density. This and the neighboring compositions also showed a favorable onset potential of 0.22 V-SCE. This was 0.15 V lower than the 0.37 V-SCE onset potential of pure Pt. These catalyst compositions exhibiting the ability to generate a stronger methanol oxidation current density at a lower potential than Pt-Ru are exciting possibilities for the next generation fuel cells.

There have been very few studies of methanol oxidation in the Pt-Ru-Co system. A few groups [58–63] have examined Pt-Co binary compositions with generally positive results. Lima et al. [43] examined Pt-Ru-W and Pt-Ru-Co catalysts electrodeposited onto a carbon support and reported that there was at least 2× improvement over Pt-Ru, but they were vague about actual compositions. Strasser et al. discovered a ternary Pt-Ru-Co alloy with promising electrocatalytic characteristics. They

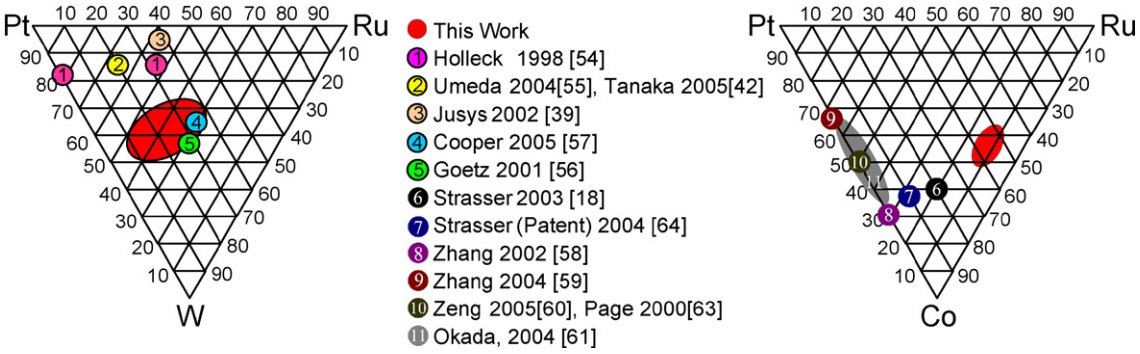

Fig. 10. Regions of the Pt-Ru-W and Pt-Ru-Co phase field that are active in the oxidation of methanol as reported by various groups.

identified $Pt_{20}Ru_{20}Co_{60}$ as being superior to the widely used $Pt_{60}Ru_{40}$ or $Pt_{50}Ru_{50}$ compositions [18]. They found that there was 4–7 times the current drawn from the cobalt containing catalyst compared to the Pt-Ru binary catalysts during the methanol oxidation. In a patent [64] of the Pt-Ru-Co system they showed an optimal composition of $Pt_{27}Ru_{10}Co_{63}$. They reported that this composition showed an improvement of 180× over their thin film $Pt_{52}Ru_{48}$ standard. When this composition was made in bulk form as a powder, they still saw a 5–10× improvement with such an alloy. The present work confirms their finding with the unconditioned $Pt_{17}Ru_{17}Co_{66}$ generating 20× more than any unconditioned Pt-Ru alloys on the same library.

4. Summary

A comparison of the optimum methanol oxidizing compositions as reported by various groups is shown in Fig. 10 for both the Pt-Ru-W and the Pt-Ru-Co phase fields. Unlike the much studied Pt-Ru binary system there is little agreement between these many reports. The optimum catalysts that we determined, $Pt_{44}Ru_{12}W_{44}$ and $Pt_{12}Ru_{50}Co_{38}$, are removed from the best compositions reported by other groups. The reason for this deviation is probably due to the differing catalysis synthesis methods with each fabrication method achieving a unique surface that makes comparison difficult.

5. Conclusions

A combinatorial system was designed to rapidly screen thin film catalyst samples for methanol oxidation. The testing successfully classified many compositions from the Pt-Ru-W and Pt-Ru-Co systems based on their short term catalysis of the methanol oxidation reaction. Catalysts that were inactive in the short timeframe test will also be inactive over longer times. These poor performing compositions have been eliminated from further consideration and will not be unnecessarily examined in a fuel cell test. Catalyst compositions that were identified as being active for methanol oxidation in the short term may be active under longer steady state conditions. This is being pursued in follow-up studies with testing of high surface area powders in a more realistic fuel cell environment.

The described thin film multiarray approach has shown its ability to compare the short term methanol oxidation of different compositions. The setup will be used to continue examining catalysts for applications in DMFC anodes. With minor modifications the multi array system can also be used to examine cathode catalysts that excel at reducing oxygen or even poison resistant catalysts for mixed reactant fuel cells.

Acknowledgements

This work was partially supported by the U.S. Army CECOM RDEC through Agreement DAAB07-03-3-K414. Such support does not constitute endorsement by the U.S. Army of the views expressed in this publication. It was also partially supported through funding from the Indiana 21st Century Technology and Research Fund.

References

[1] H.S. Liu, C.J. Song, L. Zhang, J.J. Zhang, H.J. Wang, D.P. Wilkinson, J. Power Sources 155 (2006) 95–110.
[2] E. Antolini, Mater. Chem. Phys. 78 (2003) 563–573.
[3] V. Mehta, J.S. Cooper, J. Power Sources 114 (2003) 32–53.
[4] V.S. Bagotzky, Y.B. Vassilyev, Electrochim. Acta 12 (1967) 1323–1343.
[5] M. Watanabe, S. Motoo, J. Electroanal. Chem. 60 (1975) 259–266.
[6] B.D. McNicol, R.T. Short, A.G. Chapman, J. Chem. Soc. Faraday Trans. I 72 (1976) 2735–2743.
[7] M. Watanabe, S. Motoo, J. Electroanal. Chem. 60 (1975) 267–273.
[8] D. Chu, S. Gilman, J. Electrochem. Soc. 143 (1996) 1685–1690.
[9] M.M.P. Janssen, J. Moolhuysen, Electrochim. Acta 21 (1976) 869–878.
[10] E. Reddington, A. Sapienza, B. Gurau, R. Viswanathan, S. Sarangapani, E.S. Smotkin, T.E. Mallouk, Science 280 (1998) 1735–1737.
[11] B. Gurau, R. Viswanathan, R.X. Liu, T.J. Lafrenz, K.L. Ley, E.S. Smotkin, E. Reddington, A. Sapienza, B.C. Chan, T.E. Mallouk, S. Sarangapani, J. Phys. Chem. B 102 (1998) 9997–10003.
[12] T. Iwasita, in: W. Vielstich, A. Lamm, H. Gasteiger (Eds.), Handbook of Fuel Cells: Fundamentals, Technology, Applications, Wiley, 2003, pp. 603–624.
[13] E. Antolini, J.R.C. Salgado, E.R. Gonzalez, Appl. Catal. B-Environ. 63 (2006) 137–149.
[14] T. Iwasita, Electrochim. Acta 47 (2002) 3663–3674.
[15] P. Waszczuk, A. Wieckowski, P. Zelenay, S. Gottesfeld, C. Coutanceau, J.M. Leger, C. Lamy, J. Electroanal. Chem. 511 (2001) 55–64.
[16] W.C. Choi, M.K. Jeon, Y.J. Kim, S.I. Woo, W.H. Hong, Catal. Today 93–95 (2004) 517–522.
[17] E.S. Smotkin, R.R. Diaz-Morales, Ann. Rev. Mater. Res. 33 (2003) 557–579.
[18] P. Strasser, Q. Fan, M. Devenney, W.H. Weinberg, P. Liu, J.K. Norskov, J. Phys. Chem. B 107 (2003) 11013–11021.

[19] J.F. Whitacre, T. Valdez, S.R. Narayanan, J. Electrochem. Soc. 152 (2005) A1780–A1789.
[20] S. Jayaraman, S.H. Baeck, T.F. Jaramillo, A. Kleiman-Shwarsctein, E.W. McFarland, Rev. Sci. Instrum. 76 (2005).
[21] S. Jayaraman, A.C. Hillier, Meas. Sci. Technol. 16 (2005) 5–13.
[22] Y.H. Chu, S.W. Ahn, D.Y. Kim, H.J. Kim, Y.G. Shul, H.S. Han, Catal. Today 111 (2006) 176–181.
[23] W.C. Choi, J.D. Kim, S.I. Woo, Catal. Today 74 (2002) 235–240.
[24] K. Gruber, H. Kronberger, G. Fafilek, G. Nauer, J.O. Besenhard, Fuel Cells 3 (2003) 3–7.
[25] M. Black, J. Cooper, P. McGinn, Meas. Sci. Technol. 16 (2005) 174–182.
[26] S. Guerin, B.E. Hayden, C.E. Lee, C. Mormiche, J.R. Owen, A.E. Russell, B. Theobald, D. Thompsett, J. Comb. Chem. 6 (2004) 149–158.
[27] R.X. Liu, E.S. Smotkin, J. Electroanal. Chem. 535 (2002) 49–55.
[28] B.C. Chan, R.X. Liu, K. Jambunathan, H. Zhang, G.Y. Chen, T.E. Mallouk, E.S. Smotkin, J. Electrochem. Soc. 152 (2005) A594–A600.
[29] E.S. Smotkin, J.H. Jiang, A. Nayar, R.X. Liu, Appl. Surf. Sci. 252 (2006) 2573–2579.
[30] J.S. Cooper, G.H. Zhang, P.J. McGinn, Rev. Sci. Instrum. 76 (2005).
[31] H.A. Gasteiger, N.M. Markovic, P.N. Ross, J. Phys. Chem. 99 (1995) 8290–8301.
[32] H.A. Gasteiger, N.M. Markovic, P.N. Ross, J. Phys. Chem. 99 (1995) 16757–16767.
[33] H.A. Gasteiger, N. Markovic, P.N. Ross, E.J. Cairns, J. Electrochem. Soc. 141 (1994) 1795–1803.
[34] H.A. Gasteiger, P.N. Ross, E.J. Cairns, Surf. Sci. 293 (1993) 67–80.
[35] H.A. Gasteiger, N. Markovic, P.N. Ross, E.J. Cairns, J. Phys. Chem. 97 (1993) 12020–12029.
[36] T. Biegler, D.A.J. Rand, R. Woods, J. Electroanal. Chem. 29 (1971) 269.
[37] B.E. Conway, H. Angerstein-Kozlowska, Acc. Chem. Res. 14 (1981) 49–56.
[38] R.P. Simpraga, B.E. Conway, Electrochim. Acta 43 (1998) 3045.
[39] Z. Jusys, T.J. Schmidt, L. Dubau, K. Lasch, L. Jorissen, J. Garche, R.J. Behm, J. Power Sources 105 (2002) 297–304.
[40] H.M. Saffarian, R. Srinivasan, D. Chu, S. Gilman, Electrochim. Acta 44 (1998) 1447–1454.
[41] K. Jambunathan, S. Jayaraman, A.C. Hillier, Langmuir 20 (2004) 1856–1863.
[42] S. Tanaka, M. Umeda, H. Ojima, Y. Usui, O. Kimura, I. Uchida, J. Power Sources 152 (2005) 34–39.
[43] A. Lima, C. Coutanceau, J.M. Leger, C. Lamy, J. Appl. Electrochem. 31 (2001) 379–386.
[44] J.M. Hutchinson, Platinum Met. Rev. 16 (1972) 88–90.
[45] J.B. Goodenough, R. Manoharan, Chem. Mater. 1 (1989) 391–398.
[46] A.J. Dickinson, L.P.L. Carrette, J.A. Collins, K.A. Friedrich, U. Stimming, J. Appl. Electrochem. 34 (2004) 975–980.
[47] W. Chrzanowski, A. Wieckowski, Langmuir 14 (1998) 1967–1970.
[48] A. Kabbabi, R. Faure, R. Durand, B. Beden, F. Hahn, J.M. Leger, C. Lamy, J. Electroanal. Chem. 444 (1998) 41–53.
[49] G.F. Wang, M.A. Van Hove, P.N. Ross, M.I. Baskes, Prog. Surf. Sci. 79 (2005) 28–45.
[50] J.W. Long, R.M. Stroud, K.E. Swider-Lyons, D.R. Rolison, J. Phys. Chem. B 104 (2000) 9772–9776.
[51] www.usfcc.com, Single Cell Test Protocol, US Fuel Cell Council, 2005.
[52] F.Q. Liu, C.Y. Wang, Electrochim. Acta 50 (2005) 1413–1422.
[53] A.J. Bard, L.R. Faulkner, Electrochemical Methods: Fundamentals and Applications, 2nd ed., Wiley, New York, 2001, pp. 562, 569.
[54] G.I. Holleck, D.M. Pasquariello, S.L. Clausen, Proceedings of the Second International Symposium on Proton Conducting Membrane Fuel Cells, vol. 2, 1998, pp. 150–155.
[55] M. Umeda, O. Hiroyuki, M. Mohamedi, H. Uchida, J. Power Sources 136 (2004) 10–15.
[56] M. Goetz, H. Wendt, J. Appl. Electrochem. 31 (2001) 811–817.
[57] J. Cooper, G. Zhang, P. McGinn, Proceedings for Electrochemical Society Meeting (Spring 2005), Quebec, in press.
[58] X. Zhang, K.Y. Chan, J. Mater. Chem. 12 (2002) 1203–1206.
[59] X. Zhang, K.Y. Tsang, K.Y. Chan, J. Electroanal. Chem. 573 (2004) 1–9.
[60] J.H. Zeng, J.Y. Lee, J. Power Sources 140 (2005) 268–273.
[61] T. Okada, Y. Suzuki, T. Hirose, T. Ozawa, Electrochim. Acta 49 (2004) 385–395.
[62] S.L. Gojkovic, J. Serb. Chem. Soc. 68 (2003) 859–870.
[63] T. Page, R. Johnson, J. Hormes, S. Noding, B. Rambabu, J. Electroanal. Chem. 485 (2000) 34–41.
[64] P. Strasser, Q. Fan, M. Devenney, A. Gorer, K. Cendak, K. Chondroudis, D. Giaquinta, Patent Number WO2004064181, WIPO (2004).